POAC'15
Trondheim, Norway

Proceedings of the 23rd International Conference on
Port and Ocean Engineering under Arctic Conditions
June 14-18, 2015
Trondheim, Norway

CFD SIMULATIONS OF ROLL MOTION OF A FLOATING ICE BLOCK IN WAVES USING REEF3D

Hans Bihs, Arun Kamath, Mayilvahanan Alagan Chella, Øivind A. Arntsen
Department of Civil and Transport Engineering
Norwegian University of Science and Technology, Trondheim, Norway

ABSTRACT

Floating ice blocks in waves are generally seen in managed ice and in marginal ice zones. Detailed investigations into the hydrodynamics of a floating ice block provides insight into the interaction of floating ice with arctic marine structures. In this paper, the open-source CFD code REEF3D is used to simulate the motion of a floating ice block in a wave field. The model is validated by simulating the roll motion of a rectangular barge and comparing the numerical results with experimental data. The numerical model uses the Reynolds-Averaged Navier-Stokes equations to solve the fluid flow problem. A sharp representation of the free surface is obtained using the level set method. The motion of the floating ice is calculated using the equations for six degrees of freedom motion. The floating object is immersed into the numerical grid and the solid-fluid boundary is represented with the ghost cell immersed boundary method. This method avoids re-meshing and provides increased numerical stability. Computational performance of the numerical model is improved by parallel processing using the MPI library.

INTRODUCTION

Complex floating body systems often occur in coastal, ocean and arctic engineering. In arctic engineering, one of the research applications is the behavior of floating ice blocks in a wave field. Often, this problem is combined with the interaction of fixed or floating structures, such as ships or oil platforms. In the current paper, a first attempt is undertaken towards modeling these situations with a Computational Fluid Dynamics (CFD) model. Previously, fluid-structure interaction (FSI) has been treated with Arbitrary Lagrangian-Eulerian (ALE) methods (Ramaswamy et al. (1986), Walhorn et al. (2005)). Here, the mesh follows the moving solid. In the presence of the free surface, the FSI becomes more complex. In Carrica et al. (2007), the moving solid body is captured with body conformed overset mesh. This method is more numerically robust than ALE, as constant remeshing of the solution domain can be avoided. On the other hand, overset grids require complex operations for establishing the connection between the overset mesh points and the underlying grid points in the overlapping region. The model was first presented as a one-phase model, neglecting the air-water interaction. Instead, the kinematic and dynamic boundary condition was set at the free surface boundary, which was represented by a level set function. Later, Yang et al. (2009) presented a two-phase flow version of the model using the level set method for the interface description. Their method uses a sharp interface immersed-boundary method for the solid-fluid interface without the use of an overset mesh. Based on the curvilinear immersed boundary method (Borazjani et al., 2008), Calderer et al. (2014) also present a level set based two-phase flow solver for FSI problems. In the current paper, a new six degrees of freedom (6DOF) algorithm is implemented in the open-source CFD code REEF3D (Alagan Chella et al. (2015), Kamath et al. (2015)). The complex fluid-structure interface is modeled with the ghost cell immersed boundary method (Berthelsen and

Faltinsen, 2008). Together with the staggered grid arrangement for the velocities and pressure, this leads to an accurate and stable solver for FSI problems. The model is applied to the water entry problem of a horizontal circular cylinder and the roll decay and motion of a rectangular barge and a rectangular ice block.

NUMERICAL MODEL

Governing equations

The three-dimensional numerical model presented in the paper solves the Navier-Stokes equations for mass and momentum conservation:

$$\frac{\partial u_i}{\partial x_i} = 0 \tag{1}$$

$$\frac{\partial u_i}{\partial t} + u_j \frac{\partial u_i}{\partial x_j} = -\frac{1}{\rho}\frac{\partial p}{\partial x_i} + \frac{\partial}{\partial x_j}\left[(\nu + \nu_t)\left(\frac{\partial u_i}{\partial x_j} + \frac{\partial u_j}{\partial x_i}\right)\right] + g_i \tag{2}$$

where u is the velocity averaged over time t, ρ is the fluid density, p is the pressure, ν is the kinematic viscosity, ν_t is the eddy viscosity and g the acceleration due to gravity. In order to take the effects of turbulence into account, the Reynolds-Averaged Navier Stokes (RANS) equations are solved. As a result, the two-equation $k-\omega$ model is employed (Wilcox, 1994). For the turbulent kinetic energy k and the specific turbulent dissipation ω, the following convection-diffusion equations are solved:

$$\frac{\partial k}{\partial t} + u_j \frac{\partial k}{\partial x_j} = \frac{\partial}{\partial x_j}\left[\left(\nu + \frac{\nu_t}{\sigma_k}\right)\frac{\partial k}{\partial x_j}\right] + P_k - \beta_k k\omega \tag{3}$$

$$\frac{\partial \omega}{\partial t} + u_j \frac{\partial \omega}{\partial x_j} = \frac{\partial}{\partial x_j}\left[\left(\nu + \frac{\nu_t}{\sigma_\omega}\right)\frac{\partial \omega}{\partial x_j}\right] + \frac{\omega}{k}\alpha P_k - \beta\omega^2 \tag{4}$$

With the solutions for k and ω, the relationship for the isotropic eddy viscosity becomes:

$$\nu_t = \frac{k}{\omega} \tag{5}$$

For two-phase and oscillatory flow especially, RANS turbulence models have a tendency to overestimate the turbulence production. As a countermeasure, the eddy viscosity is kept bounded (Durbin, 2009) and additional free surface turbulence dissipation is added to the standard model (Naot and Rodi, 1982).

The pressure term in Eq. 2 is solved with the projection method (Chorin, 1968) for incompressible flow. The resulting Poisson equation for the pressure is solved iteratively with the preconditioned BiCGStab solver (van der Vorst, 1992). The model is fully parallelized with the domain decomposition method and MPI. REEF3D has been tested and validated on the high performance computing systems at NTNU in Trondheim (NOTUR, 2015) and shows very good scaling properties. The convective terms of all transport equations are discretized with the conservative finite difference Weighted Essentially Non-Oscillatory (WENO) scheme (Jiang and Shu, 1996), with the exception of the level set equation, where the Hamilton-Jacobi version of WENO is employed (Jiang and Peng, 2000). For time discretization, a second-order TVD Runge-Kutta scheme is used (Shu and Osher, 1988). The numerical model uses a Cartesian grid and complex geometries are handled with a ghost cell immersed boundary method (Berthelsen and Faltinsen, 2008).

Free Surface

In REEF3D, the free surface is modeled with the interface capturing level set method (Osher and Sethian, 1988). The parameter $\phi(\vec{x},t)$ is a signed distance function, giving the closest distance to the interface between two fluids in the whole solution domain (Eq. 6). The different fluids are distinguished by either a positive or negative sign.

$$\phi(\vec{x},t)\begin{cases} >0 & if\ \vec{x}\ is\ in\ phase\ 1 \\ =0 & if\ \vec{x}\ is\ at\ the\ interface \\ <0 & if\ \vec{x}\ is\ in\ phase\ 2 \end{cases} \tag{6}$$

The interface between the two fluids is coupled to the external velocity field through a convection equation for the level set function (Eq. 7). After convection, the new level set function does not necessarily adhere to the signed distance requirement. In order to maintain this property throughout the simulation, the level set function is reinitialized after every time step (Peng et al., 1999). The changes of the interface location are considered by the flow solver by using updated density and viscosity values for each grid point, depending on the fluid phase.

$$\frac{\partial \phi}{\partial t} + u_j \frac{\partial \phi}{\partial x_j} = 0 \tag{7}$$

The numerical model has the capabilities to generate and dissipate waves. For this, the relaxation method is used Jacobsen et al. (2011). High quality waves based on wave theory or irregular wave spectra can be generated in the relaxation zone. There, the values for the velocities and the free surface are ramped up from the actual computational values to the prescribed values. Reflections from the downstream boundary can pollute the numerical simulation in the wave tank. In order avoid this, the relaxation method is used to smoothly transition the velocity, free surface and pressure to the values corresponding to still water level conditions.

6DOF algorithm

A free floating body has six degrees of freedom, the translation consisting of the three linear velocities $u, v,$ and w and the rotation with the three angular velocities $p, q,$ and r (Fossen, 1994). The location and the orientation of the floating body are given by the position vector and the Euler angles:

$$\boldsymbol{\eta} = (\boldsymbol{\eta}_1, \boldsymbol{\eta}_2) = (x_c, y_c, z_c, \phi, \theta, \psi) \tag{8}$$

As the floating body is moving and rotating, its orientating is dynamically changing in respect to the underlying numerical mesh. It is convenient to introduce two separate coordinate systems: The inertial coordinate system in which the fluid flow is calculated, and the non-inertial coordinate system for the floating body. Then the forces X, Y and Z and moments K, M and N acting on the body can be calculated in the inertial coordinate system in a straightforward manner. The forces acting on the surface Ω of the floating body can be determined for each coordinate direction i separately in the following way:

$$F_i = \int_\Omega (-\mathbf{n}_i p + \mathbf{n}_i \cdot \tau) d\Omega \tag{9}$$

The momentum is determined as follows:

$$M_i = \int_\Omega \mathbf{r} \times (-\mathbf{n}_i p + \mathbf{n}_i \cdot \tau)\, d\Omega \tag{10}$$

The vector $\mathbf{r}$ is the distance of each surface element of the floating body to the center of gravity, which is determined with Eq. 11.

$$\mathbf{r}_{cg} = \frac{1}{m} \int_V \mathbf{r}\, \rho_a\, dV \tag{11}$$

Based on the Euler angles, the calculated forces and moments can be expressed in the non-inertial coordinate system with a rotation matrix $\mathbf{J}_1^{-1}$, consisting of three elemental rotations around the axis of the coordinate system (s stands for sin and c for cos):

$$\boldsymbol{a}_{fb} = \begin{bmatrix} c\phi\, c\theta & s\phi\, c\theta & -s\theta \\ -s\psi\, c\phi + s\phi\, s\theta\, c\psi & c\psi\, c\phi + s\phi\, s\theta\, s\psi & s\phi\, c\theta \\ s\theta\, s\psi + c\phi\, s\theta\, c\psi & -s\phi\, c\psi + c\phi\, s\theta\, s\psi & c\theta\, c\phi \end{bmatrix} \boldsymbol{a}_e = \mathbf{J}_1^{-1}\, \boldsymbol{a}_e \tag{12}$$

Here $\boldsymbol{a}_{fb}$ is a vector in the reference frame of the floating body, and $\boldsymbol{a}_e$ a vector in the inertial coordinate system. The usage of two different coordinate systems also simplifies the computation of the solid body parameters. When the origin of the non-inertial coordinate system coincides with the center of gravity, the moments of inertia can be calculated in a straightforward manner:

$$\mathbf{I} = \begin{bmatrix} I_x & 0 & 0 \\ 0 & I_y & 0 \\ 0 & 0 & I_z \end{bmatrix} = \begin{bmatrix} mr_x^2 & 0 & 0 \\ 0 & mr_y^2 & 0 \\ 0 & 0 & mr_z^2 \end{bmatrix} \tag{13}$$

With the calculation of the forces, momentum and moments of inertia in place, the dynamic rigid body equations can be solved (Carrica et al., 2007):

$$\begin{aligned} [m(\dot{u} - vr + wq)] &= X - Cu \\ [m(\dot{v} - wp + ur)] &= Y - Cv \\ [m(\dot{w} - uq + vp)] &= Z - Cw \\ [I_x\dot{p} + (I_z - I_y)qr] &= K - Cp \\ [I_y\dot{q} + (I_x - I_z)rp] &= M - Cq \\ [I_z\dot{r} + (I_y - I_x)pq] &= N - Cr \end{aligned} \tag{14}$$

Here u, v, w, p, q and r are the values for the linear and angular velocities from the previous time step and C the damping coefficent. Then $\dot{u}, \dot{v}, \dot{w}, \dot{p}, \dot{q}$ and $\dot{r}$ can be calculated in an explicit manner. Then any of the linear and angular velocities $\dot{\varphi}$ and consecutively any component of the position and orientation vector φ of the floating body can be explicitly calculated with a second-order Adams-Bashforth scheme for the new time step:

$$\begin{aligned} \dot{\varphi}^{n+1} &= \dot{\varphi}^n + \frac{\Delta t}{2}\left(3\ddot{\varphi}^{n+1} - \ddot{\varphi}^n\right) \\ \varphi^{n+1} &= \varphi^n + \frac{\Delta t}{2}\left(3\dot{\varphi}^{n+1} - \dot{\varphi}^n\right) \end{aligned} \tag{15}$$

As the dynamic rigid body equations have been solved in the floating body reference frame, also the translations and and orientations are calculated there. They need to be transformed to the inertial reference frame. For the translations, the matrix given in Eq. 12 is used. The angles are transformed using the rotation matrix $\mathbf{J}_2$ (Fossen, 1994):

$$\dot{\boldsymbol{\eta}}_2 = \begin{bmatrix} 1 & sin\phi\, tan\theta & cos\phi\, tan\theta \\ 0 & cos\phi & -sin\phi \\ 0 & sin\phi/cos\theta & cos\phi/cos\theta \end{bmatrix} \boldsymbol{v}_2 = \mathbf{J}_2\, \boldsymbol{v}_2 \tag{16}$$

Then the position and orientation of the floating body is updated. In REEF3D, the geometry of the moving floating body is handled with a triangular surface mesh. Intersections with the underlying Cartesian grid are determined with a ray-tracing algorithm (Yang and Stern, 2014). When the rigid body is moving through the flow field, this movement is taken into account by setting the body velocity resulting from translation and rotation as a boundary condition on the solid-fluid interface:

$$U_i = \dot{\boldsymbol{\eta}}_\mathbf{1} + \dot{\boldsymbol{\eta}}_\mathbf{2} \times \mathbf{r} \tag{17}$$

RESULTS

Water Entry Problem

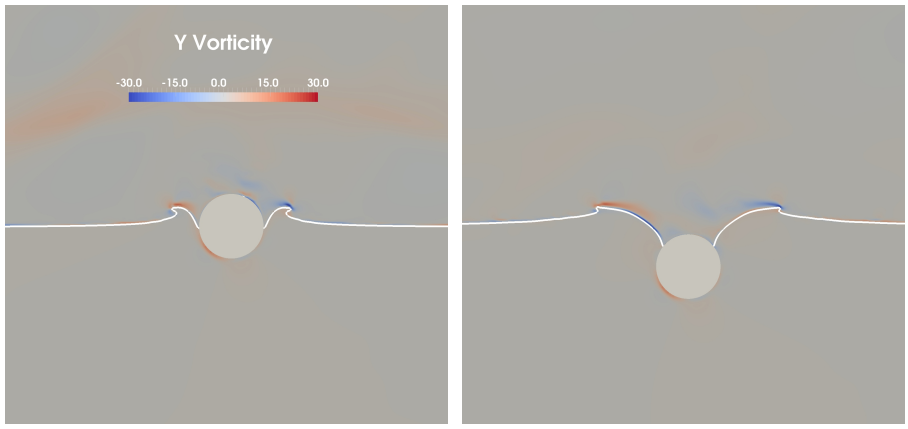

(a) T=1.0 (b) T=2.0

(c) T=3.0 (d) T=4.0

Figure 1: Disc entry problem, the contour shows the vorticity.

The performance and numerical stability of the 6DOF algorithm is shown with a numerical benchmark case. The water entry problem of a horizontal circular cylinder has been simulated by several authors (Yang et al. (2009) or Calderer et al. (2014)). All parameters of this test are non-dimensional. The disc enters the water with the fixed vertical velocity of $V = -1$. The center of the disc is located $H = 1.25$ over the free surface at $T = Vt/H = 0$. The cylinder has a radius of $R = 1$. The two-dimensional simulation domain has the size $30R \times 22R$. The uniform mesh size is $dx = 0.025$, resulting in 1200×880 grid cells. Gravity is set to $g = -1$, the density of the water to $\rho_{water} = 1$, the density of the air to $\rho_{air} = 0.001$, the viscosity of the water to $\nu_{water} = 0.001$ and the viscosity of the air to $\nu_{air} = 0.018$. The time step size is controlled with adaptive time stepping using a CFL number of 0.1. The free surface location and the vorticity contour are shown in Fig. 1. In Fig. 1a, the horizontal cylinder has started to enter the body of water. On both sides of the cylinder, breaking waves can be observed. As reported earlier (Calderer et al., 2014), capturing the breaking waves requires a sufficiently fine mesh. At $T = 1.0$, the waves generated by the disc impact are propagating towards the outer side of the domain. In Fig. 1c, the horizontal cylinder is fully submerged. Due to the downward directed cylinder motion, the free surface elevation over the disc is distinctly lowered. Later, at $T = 4.0$, the cylinder is more than one full radius R away from the free surface. The water from the sides is returning to the area on top of the cylinder and creates a vertical water jet. The model was numerically stable throughout the simulation and the free surface location compares fairly well with other results reported in literature.

Roll Motion Barge and Ice

The case of roll motion of a rectangular barge in waves has been presented by Jung et al. (2006). They performed experiments in a wave flume with the barge fixed around the rotational direction axis in the center of gravity of the structure, resulting in a single degree of freedom. The barge is 0.3 m long, 0.1 m high and 0.9 m wide. It is made of solid acrylic glass with the density $\rho = 1048$ kg/m^3, resulting in a momentum of inertia $I_y = 0.236$ kg m^2 for the direction of the roll motion.

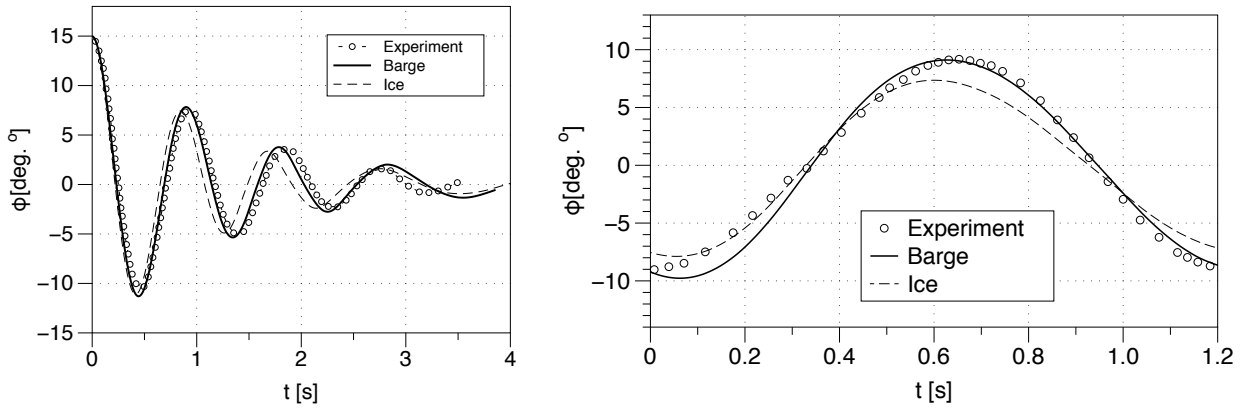

(a) Roll decay

(b) Roll motion under waves

Figure 2: Roll motion of a rectangular barge and a rectangular block of ice.

The wave flume is 0.9 m wide and has a water depth of $h = 0.9$ m. For the freshwater in the wave tank, a density of $\rho = 998.2$ kg/m^3 is used. The center of gravity of the barge coincides with the still

water free surface location. In addition to the structure used in the experiments, the same tests as in Jung et al. (2006) are numerically performed for a rectangular block of sea ice with the density of $\rho = 900$ kg/m^3 in salt water with the density of $\rho = 1025$ kg/m^3. Thus, in contrast to the experimental conditions, in the case of the ice the rectangular structure is lighter than the surrounding fluid.

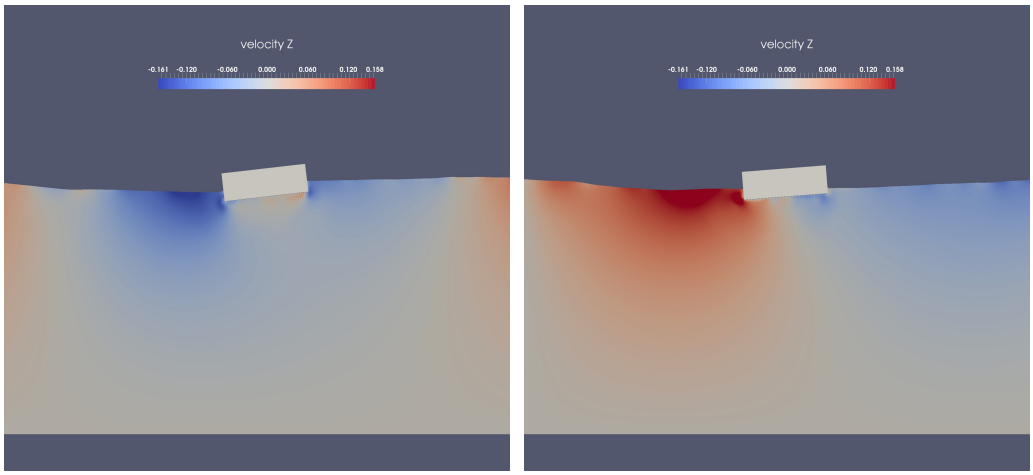

(a) t = 0.0 s

(b) t = 0.3 s

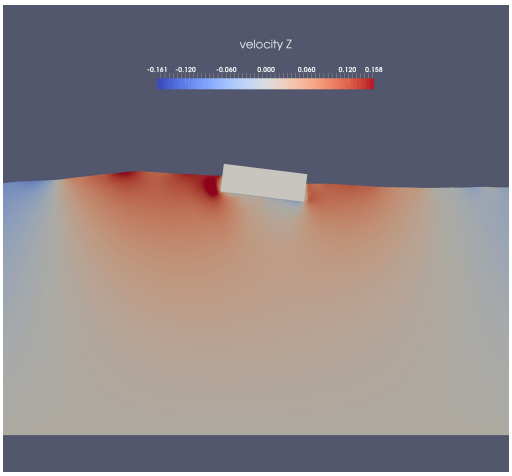

(c) t = 0.6 s

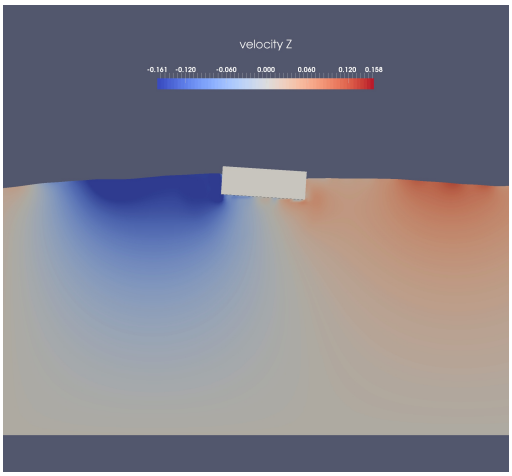

(d) t = 0.9 s

Figure 3: Roll motion of the rectangular barge, the contour shows the vertical velocity.

At first, a roll decay test is performed. The barge is initially tilted to an angle of $15°$ and then released. The roll angle is recorded with a rotary position sensor in the experiments. In the numerical simulations the case is treated as two-dimensional, as it is symmetric along the width. The numerical domain for the roll decay test is 5 m long and 1.6 m high, the inflow and outflow boundaries are modeled as walls. A uniform mesh size of $dx = 0.01$ m is used, resulting in a moment of inertia of $I_y = 0.0026$ kg m^2 for the 0.01 m wide barge. Following Calderer et al. (2014), the damping coefficient of $C = 0.003$ (corresponding to $C = 0.275$ in 3D) is used in the rigid body equations, in order to account for the friction of the experimental apparatus. Fig. 2a shows the comparison between the experimental and numerical results for the roll decay test. For the acrylic glass barge,

the calculated roll angle ϕ agrees well with measurements up to around 3 s. After that, the numerical results go out of phase, as the generated water waves are reflected back towards the barge from the up- and downstream walls. It is expected, that extending the flow domain will result in a better agreement at the later stages of the roll decay test. For the rectangular block of ice, the structure moves at a slightly faster rate with a minimal reduction of the amplitude for ϕ. This can be credited to the lower density of the ice and the resulting lower moment of inertia I_y.
Next, the behavior of the rectangular barge under the influence of regular periodic waves is investigated. Waves with a length of $L = 2.2$ m, a wave period of $T = 1.2$ s and a height $H = 0.06$ m are generated. The simulation domain has the length $L = 12$ m, the wave generation zone is 2.2 m long and the numerical beach is 4.4 m long. Fig. 2b shows the roll angle over one wave period. Again, the comparison between the numerical model and the experiment for the roll angle ϕ shows good agreement. For the rectangular block of ice the magnitude of the roll angle is reduced by about $3°$. Fig. 3 shows the acrylic glass barge for different stages over one wave period without the air phase. The contour shows the vertical velocity.

CONCLUSIONS

In the current paper, the new six degree of freedom (6DOF) algorithm implemented in the open-source CFD code REEF3D is presented. The model solves the Reynolds-Averaged Navier-Stokes equations for the flow and uses the level set method for the capturing of the free surface. Waves are generated with the relaxation method. For a moving structure inside the fluid, the dynamic rigid body equations are solved. The solid-fluid interface is treated with the ghost cell immersed boundary method. The model is first applied to the benchmark case of the water entry problem of a horizontal circular cylinder. The test reveals the good numerical stability of the algorithm, and the location of the free surface corresponds well with results reported in literature. Next, the roll decay and the roll motion for waves of a rectangular barge are modeled. The simulated roll angles agree well with the experimental data. The same tests are performed numerically for a rectangular block of ice with the same geometry as the barge. Small differences in the roll motion due to the different density of the structures are observed. Overall, the 6DOF model performed well and has the potential to solve complex fluid-structure interaction problems related to arctic engineering.

References

Alagan Chella, M., Bihs, H., Myrhaug, D., and Muskulus, M. (2015). "Breaking characteristics and geometric properties of spilling breakers over slopes." *Coastal Engineering*, 95, 4–19.

Berthelsen, P. A. and Faltinsen, O. M. (2008). "A local directional ghost cell approach for incompressible viscous flow problems with irregular boundaries." *Journal of Computational Physics*, 227, 4354–4397.

Borazjani, I., Ge, L., and Sotiropoulos, F. (2008). "Curvilinear immersed boundary method for simulating fluid structure interaction with complex 3d rigid bodies." *Journal of Computational Physics*, 227, 7587–7620.

Calderer, A., Kang, S., and Sotiropoulos, F. (2014). "Level set immersed boundary method for coupled simulation of air/water interaction with complex floating structures." *Journal of Computational Physics*, 277, 201–227.

Carrica, P. M., V., W. R., Noack, R. W., and Stern, F. (2007). "Ship motions using single-phase level set with dynamic overset grids." *Computer Fluids*, 36, 1415–1433.

Chorin, A. (1968). "Numerical solution of the Navier-Stokes equations." *Mathematics of Computation*, 22, 745–762.

Durbin, P. A. (2009). "Limiters and wall treatments in applied turbulence modeling." *Fluid Dynamics Research*, 41, 1–18.

Fossen, T. I. (1994). *Guidance and Control of Ocean Vehicles*. John Wiley Sons.

Jacobsen, N. G., Fuhrman, D. R., and Fredsøe, J. (2011). "A wave generation toolbox for the open-source CFD library: OpenFOAM." *International Journal for Numerical Methods in Fluids*, 70(9), 1073–1088.

Jiang, G. S. and Peng, D. (2000). "Weighted ENO schemes for Hamilton Jacobi equations." *SIAM Journal of Scientific Computing*, 21, 2126–2143.

Jiang, G. S. and Shu, C. W. (1996). "Efficient implementation of weighted ENO schemes." *Journal of Computational Physics*, 126, 202–228.

Jung, K. H., Chang, K.-A., and Jo, H. J. (2006). "Viscous effect on the roll motion of a rectangular structure." *Journal of Engineering Mechanics*, 132(2), 190–200.

Kamath, A., Bihs, H., and Arntsen, Ø. A. (2015). "Numerical modeling of power take-off damping in an oscillating water column device." *International Journal of Marine Energy*, 10, 1–16.

Naot, D. and Rodi, W. (1982). "Calculation of secondary currents in channel flow." *Journal of the Hydraulics Division, ASCE*, 108(8), 948–968.

NOTUR (2015). "Notur - the Norwegian Metacenter for Computational Science.

Osher, S. and Sethian, J. A. (1988). "Fronts propagating with curvature-dependent speed: Algorithms based on Hamilton-Jacobi formulations." *Journal of Computational Physics*, 79, 12–49.

Peng, D., Merriman, B., Osher, S., Zhao, H., and Kang, M. (1999). "A PDE-based fast local level set method." *Journal of Computational Physics*, 155, 410–438.

Ramaswamy, B., Kawahara, M., and Nakayama, T. (1986). "Lagrangian finite element method for the analysis of two-dimensional sloshing problems." *International Journal for Numerical Methods in Fluids*, 6, 659–670.

Shu, C. W. and Osher, S. (1988). "Efficient implementation of essentially non-oscillatory shock capturing schemes." *Journal of Computational Physics*, 77, 439–471.

van der Vorst, H. (1992). "BiCGStab: A fast and smoothly converging variant of Bi-CG for the solution of nonsymmetric linear systems." *SIAM Journal of Scientific Computing*, 13, 631–644.

Walhorn, E., Kölke, A., Hübner, B., and Dinkler, D. (2005). "Fluid–structure coupling within a monolithic model involving free surface flows." *Computer Structures*, 83, 2100–2111.

Wilcox, D. C. (1994). *Turbulence Modeling for CFD*. DCW Industries Inc., La Canada, California.

Yang, J. and Stern, F. (2014). "Robust and efficient setup procedure for complex triangulations in immersed boundary simulations." *Journal of Fluids Engineering*, 135(10), 101107.1–101107.11.

Yang, J., Wang, Z., and Stern, F. (2009). "Sharp interface immersed-boundary/level-set method for wave–body interactions." *Journal of Computational Physics*, 228, 6590–6616.